AL-Bahir
Journal for Engineering and Pure Sciences
BJEPS

Volume 7 | Issue 1 Article 3

An Integrated Geophysical Approach for Estimating the Depth of Mineral Potential in Some Part of Basement Complex Terrain Southwestern Nigeria

Hamid Titilope Oladunjoye
Department of Physics, Olabisi Onabanjo University, Ago Iwoye, Ogun State, Nigeria

Joseph Coker
Department of Physics, Olabisi Onabanjo University, Ago Iwoye, Ogun State, Nigeria

Niyi-Ola Adebisi
Department of Earth Sciences, Olabisi Onabanjo University, Ago-Iwoye, Ogun State, Nigeria

Omolara Abosede Adenuga
Department of Physics, Olabisi Onabanjo University, Ago Iwoye, Ogun State, Nigeria

Sofiat Adetomilola Adekoya
1Department of Physics, Olabisi Onabanjo University, Ago Iwoye, Ogun State, Nigeria

See next page for additional authors

Recommended Citation

Oladunjoye, Hamid Titilope; Coker, Joseph; Adebisi, Niyi-Ola; Adenuga, Omolara Abosede; Adekoya, Sofiat Adetomilola; Alabi, Aderemi; and Akinmoladun, Abisola (2025) "An Integrated Geophysical Approach for Estimating the Depth of Mineral Potential in Some Part of Basement Complex Terrain Southwestern Nigeria," *Al-Bahir*: Vol. 7: Iss. 1, Article 3.
Available at: https://doi.org/10.55810/2313-0083.1103

An Integrated Geophysical Approach for Estimating the Depth of Mineral Potential in Some Part of Basement Complex Terrain Southwestern Nigeria

Authors

Hamid Titilope Oladunjoye, Joseph Coker, Niyi-Ola Adebisi, Omolara Abosede Adenuga, Sofiat Adetomilola Adekoya, Aderemi Alabi, and Abisola Akinmoladun

Source of Funding

This research received no external funding.

Conflict of Interest

The authors do not have any conflict of interest to declare.

Data Availability

The data supporting the findings of this study are presented in the manuscript. The raw datasets or analysis outputs are available on request.

ORIGINAL STUDY

An Integrated Geophysical Approach for Estimating the Depth of Mineral Potential in Some Part of Basement Complex Terrain, Southwestern Nigeria

Hamid T. Oladunjoye [a,*], Joseph Coker [a], Niyi-Ola Adebisi [b], Omolara A. Adenuga [a], Sofiat A. Adekoya [a], Aderemi Alabi [c], Abisola Akinmoladun [a]

[a] Department of Physics, Olabisi Onabanjo University, Ago Iwoye, Ogun State, Nigeria
[b] Department of Earth Sciences, Olabisi Onabanjo University, Ago-Iwoye, Ogun State, Nigeria
[c] Department of Physics, Federal University of Agriculture, Abeokuta, Ogun State, Nigeria

Abstract

Effective mineral exploration in a basement complex necessitates precise delineation of overburden thickness and mineral potential within the Basement Complex terrain. This study examined the subsurface geology and assesses the abundance of prospective mineral deposits within the study area. The objective of the study was to outline the overburden thickness and infer mineral potential using integrated ground magnetic and electrical resistivity geophysical methods. The electrical resistivity method unraveled the litho-stratigraphic sequence as surmised from geo-electric layers. Consequently, the mineralization of the basement delineated was characterized by the magnetic method. The acquired data were processed using WINRESIST and Oasis Montaj respectively. The electrical resistivity method provided detailed litho-stratigraphic information, revealing geo-electric layers corresponding to the topsoil (302−933 Ωm), weathered layer (48−181 Ωm), and bedrock (421−1357 Ωm), with overburden thicknesses ranging between 7.62 m and 9.5 m. Ground magnetic data further characterized the basement mineralization, identifying three distinct magnetic anomalies: a null anomaly district (−3 to 3 nT), a weak positive anomaly (7.3−12.4 nT), and a magnetic closure (17.7−22 nT). Magnetic source depths varied between 1 m and 14 m, with low magnetic susceptibility indicative of porphyritic granite with quartz phenocrysts. In conclusion, the findings are particularly favorable for quarrying operations in the northern sector of the study area, where granite abundance is estimated at around 68 %, indicating strong economic potential. This integrated approach of electrical and magnetic geophysical methods, described the accuracy of subsurface mapping by simultaneously resolving overburden thickness and inferring mineral potential in a Basement Complex terrain.

Keywords: Geo-electric, Granite, Magnetic, Porphyritic, Regolith

1. Introduction

Geophysical techniques have been proven to be a powerful tool in estimation of potential zone for mineral deposits with its associated characteristics such as volume, depth, direction of concentration with respect to faults and fracture line associated with it [1]. The Earth surface contributes to the profound civilization and development through the provision of enable inhabitancy. Human development has depended heavily on resources obtained from both near surface (as in construction material) and hundreds to thousands of meters deep surface such as groundwater, metalliferous ores and petroleum-based products [2,3]. The water from a high yield aquifer is useful for domestic and commercial purposes. Similarly, most nations such as Nigeria based their source of income on the ores

Received 21 February 2025; revised 19 May 2025; accepted 28 May 2025.
Available online 19 June 2025

* Corresponding author.
E-mail addresses: oladunjoye.titilope@oouagoiwoye.edu.ng (H.T. Oladunjoye), coker.joseph@oouagoiwoye.edu.ng (J. Coker), niyiola.adebisi@oouagoiwoye.edu.ng (N.-O. Adebisi), adenuga.omolara@oouagoiwoye.edu.ng (O.A. Adenuga), adekoya.sofiat@oouagoiwoye.edu.ng (S.A. Adekoya), aderemi.alabi@funaab.edu.ng (A. Alabi), abisola.akin@oouagoiwoye.edu.ng (A. Akinmoladun).

https://doi.org/10.55810/2313-0083.1103

extracted beneath the earth surface for their sustainability [4].

The basement complex region of Nigeria is rich in minerals that hold both domestic and commercial significance [5,6]. The basement complex of Nigeria is characterized as a hybrid assemblage of igneous and metamorphic rocks with minerals comprising of quartz, tridymite, cristobalite, feldspathoids, muscovite, and corundum. The array of these minerals is divided into two viz; felsic mineral-rich and mafic mineral-rich. The former comprises of feldspar and silica while latter comprises of magnesium and ferrous iron. The crystalline rocks constitute the basement complex of Nigeria covering about half of the country's landmass which is classified broadly into three; namely; the gneiss-migmatite complex, the meta-sedimentary schist belt and the older granite. These minerals are characterized with a lot of usefulness for domestic and commercial purposes [7,8]. The usefulness of granite in the construction of buildings, roads and bridges are enormous, thereby commercial importance of its mining has increased tremendously. The study was carried out within Odeda axis of the Southwestern Basement of Nigeria is characterized with basement rock that is rich with mineral deposit. The basement rocks found in the study are mainly intrusive -buried underneath the Earth surface. This implies that, the details of the lithostratigraphic sequence are required in order to characterize the overburden to the basement or potential minerals.

In a bid to unravel the minerals within the subsurface, detailed information and characteristics of the minerals are important. This will inform about the specifics of its location, distribution, depth and structure of surrounding rock with respect to their porosity and permeability. The earth inherent complexity can make it difficult and impossible to infer these characteristics from direct observation. Therefore, these characteristics and features are often inferred from the analysis and interpretation of fundamental physical properties such as density, electrical conductivity, magnetic susceptibility, and acoustic impedance that are related to the mineral as obtained and inferred from the measured geophysical parameters [9,10].

Odeda Local Government Area (LGA), situated within the Precambrian Basement Complex of southwestern Nigeria, which composed of ancient crystalline rocks with diverse mineral deposits [11,12]. Neighboring towns such as Abeokuta North & South, Obafemi Owode, Ewekoro, and Ifo also host various valuable mineral deposits. Abeokuta North & South, for instance, is known for its granite, kaolin, and feldspar, which support the construction and ceramics industries [12]. In Ewekoro, limestone is abundant and mainly used in cement production, while phosphate and gypsum are also present, contributing to the fertilizer and construction industries [12]. Similarly, towns like Sagamu and Ifo are rich in limestone, kaolin, feldspar, and silica sand, which further emphasize the region's potential for industrial applications, particularly in cement and ceramics.

Geophysical surveys have been conducted across Odeda and neighboring areas, providing valuable insights into subsurface mineralization [13,14]. Although these studies have facilitated the identification of mineral deposits, detailed quantitative estimation of the mineral resources has yet to be thoroughly carried out.

The Electrical Resistivity Tomography (ERT) is one of the proven tools used for unravelling the stratigraphy and lithological arrangement of the overburden in basement complex. Resistivity surveys measure variation in the electrical resistivity of the ground by applying small electric current across arrays of ground electrodes [15]. Few studies from Refs. [9,10,16] have shown the veracity of the usefulness of different techniques in unravelling the lithostratigraphic sequence within the subsurface. The magnetic method has demonstrated its effectiveness in mineral exploration by identifying structures that host ore and determining sediment thickness (depth to the sources of anomalies), while also acting as a preliminary tool for structural characterization for possible mineral deposit. Researchers such as [17–19] have demonstrated the veracity of the usefulness of magnetic method in location of near surface faults, igneous dikes and studied tomographic objects like storage drums, pipes, artifacts, etc. The analysis and localization of the magnetic signature depends solely on the depth to the basement and its makeup since a non-magnetic body is completely unable to be detectable [4,20–22].

The study investigated the subsurface thickness representing the overburden to potential mineral deposit while the estimation of the bulk density of the minerals is assessed within the study area. The integrated geophysical approach comprising of ground magnetic and electrical resistivity methods is capable of delineating, unravelling and showing the distribution of the lithostratigraphic sequence of the study area. Also, the mineral composition of the delineated rocks will suggest the bulk density and its abundance for possible economic value.

2. Materials and methods

2.1. Location and geology of the study area

The study area is located on the outskirts of Abeokuta, an ancient city in the Southwestern part of Nigeria. It is situated approximately between latitude 7° 22′ 59″ and 3° 54′ 45″E and on the longitude 7° 92′ 64″ and 3° 86′ 90″N of the Greenwich meridian. The study area is found within the crystalline basement complex of Southwestern Nigeria. The entire community covers an area extent of approximately 1560 km^2, with densely vegetation comprising of highway, major roads, rail roads and foot path as depicted [23] in Fig. 1. The study area is characterized by a tropical climate with distinct wet and dry seasons. The wet season is associated relatively with the prevalence of the Moist Maritime Southerly Monsoon from the Atlantic Ocean and dry season is associated with the Continental North Easterly Harmattan winds from Sahara Desert. The area is located within a region characterized by bimodal rainfall pattern (commences in March and is plentiful in July and September, with a short dry spell in August). The long dry period extends from November to March [24].

The study area falls within the Basement Complex of Nigeria as shown in Fig. 1. Previous scientists identified the rocks within the study area as mainly metamorphic rocks of gneiss family which can further be classified into Porphyroblastic gneiss, Quartzite schist, Banded gneiss, and Hornblende-Biotite granite [25]. Porphyroblastic gneiss are not completely foliated as the light band forms larger phenocryst that are aligned in the same direction but not completely stretched. They contain both mafic and felsic minerals like quartz, biotite, muscovite, and plagioclase feldspar. Also, Quartzite schist comprising of metamorphosed schist composed mostly of quartz with some mica and/or tourmaline [6,25,26].

However, Banded gneiss is foliated metamorphic rocks which are rich in felsic and mafic minerals form a distinct band of colors from which the name banded gneiss is derived. They occur in bands of dark and light-colored minerals [27]. The study area is linked with minor and major roads as depicted in Fig. 2. The main settlement (Odeda) in the area is described with major amenities to be regarded to as city. The neighboring cities that are linked with major and minor road are settlement characterized with farming activities.

2.2. Data acquisition

Schlumberger configuration of Vertical Electrical Sounding (VES) was employed as a resistivity method in delineating the subsurface information of the study area.

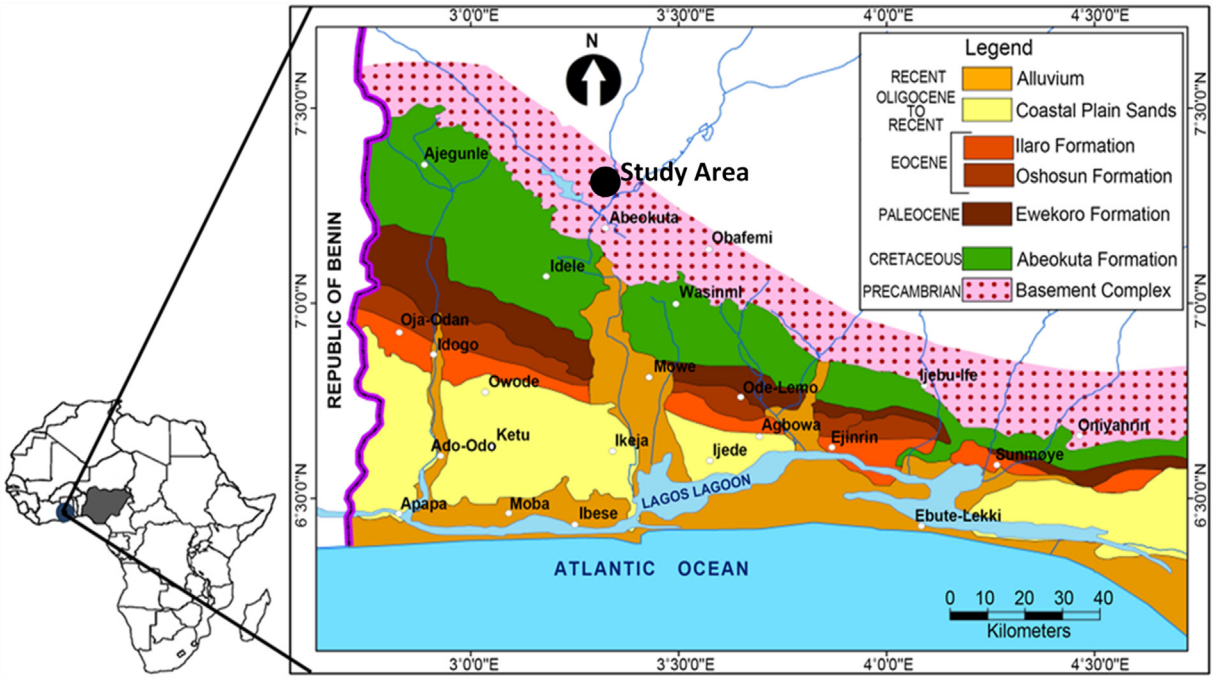

Fig. 1. Map showing the study area.

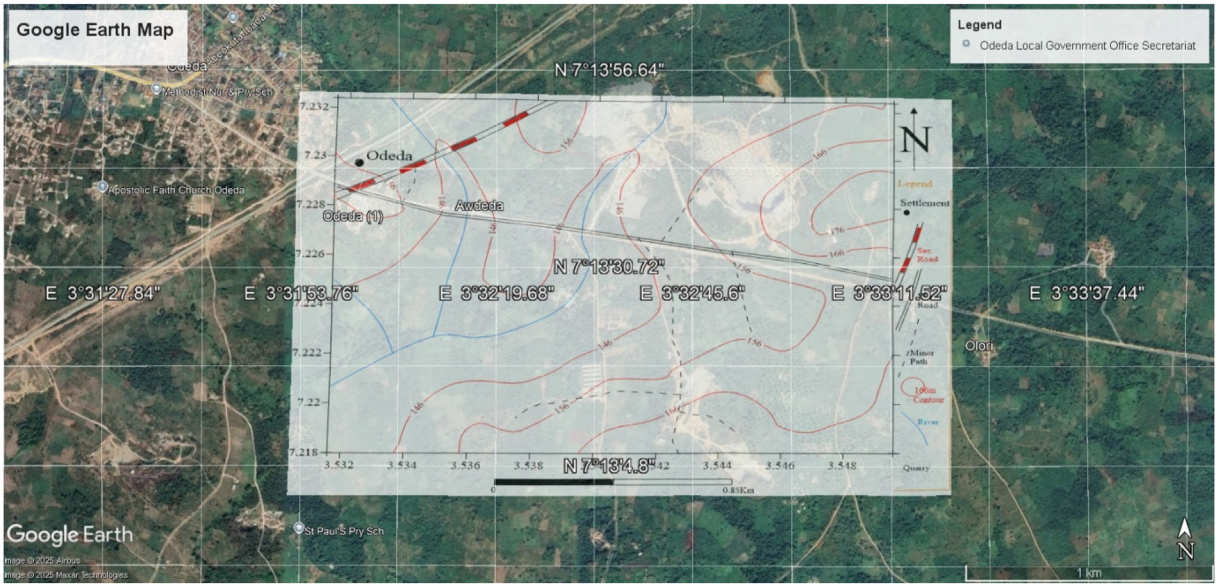

Fig. 2. Topographical map of the study area.

From the acquired electric resistivity data, geo-electric parameters and geo-section layers could be obtained in order to characterize the lithological sequence of the study area. The overburden thickness representing the regolith to the potential mineral deposit and basement in the study area were obtained. Likewise, the processed magnetic data revealed the source-depth information of the magnetic source. The magnetization of the mineral informed about the source and the depth which gives the mineral potential and their respective depths. Both methods unraveled the depth to basement complex and mineral deposits, while electrical resistivity depicts that inform of geo-electric section/layers, magnetic methods employs low or high magnetic signals for its delineation. Ref. [28] explored the groundwater using the magnetic and electrical methods to identify the structure and depth to the magnetic sources and possible faults that may affect the groundwater flow. The correlation between these methods provides valuable information of magnetic intensity and depth for potential groundwater resources of the study area.

Thirty (30) VES was carried out with current electrodes array (AB/2) ranging from 400 to 500 m. The ABEM Terrameter SAS 1000, a digital resistivity meter designed for geo-electrical investigations, was employed for data acquisition in this study, along with its standard accessories, including electrodes, metallic clips, connecting wires, and hammers. The terrameter is renowned for its high resolution, portability, and capability to investigate exploration, geotechnical, and hydrogeological studies. The system aids effective ground contact and ensures accurate measurement of subsurface resistivity by connecting wires and clips that link the electrodes to the Terrameter. The Terrameter injects electrical current into the subsurface through the current electrodes and measures the resulting potential difference via the potential electrodes, thus presenting the equivalent resistance values. The apparent resistivity is calculated by multiplying the geometry factor K with the resistance measured by the Terrameter relationship using Equation (1).

$$\ell = KR \tag{1}$$

Where,

K = Geometric factor; R = Resistance; ℓ = Apparent resistivity.

The acquisition set up was designed in such a way that the current and potential electrodes were progressively set out to achieve a well-defined profile during which the current electrode was ensured to be five times of the potential electrode at the start. As the current electrode separation increase progressively the potential electrodes remain constant until potential reading become small to be measured. Schlumberger sounding has better resolution, greater probing depth, and less time-consuming when compared to Wenner array.

Magnetic geophysical method is used to investigate subsurface structures by measuring variations in the Earth's magnetic field. These variations often

arise from changes in the magnetic properties of underlying rocks. Prior to the commencement of the data acquisition, the survey mode was designed, and the data acquisition technique suitable for the study objectives was identified. Careful planning of the survey geometry is also crucial. Magnetic sensors should be held at a constant height above the ground and moved steadily along predefined lines to reduce inconsistencies caused by jerky motion or uneven elevation. Cultural noise emanating from power lines, fences, pipelines, and vehicles should be minimized by conducting surveys away from such interference zones [14]. The Magnetic method is conducted in either grid or traverse patterns, depending on the geological objective. For the purpose of this study, data was acquired in grid pattern (Fig. 3) to achieve high spatial resolution of the subsurface features. To enhance accuracy in data acquisition, magnetic data was acquired in survey mode. Data was collected at specific predetermined points of 5 m apart along the grid.

The GEM 19T Proton Precession Magnetometer was utilized for the acquisition of geophysical magnetic data, along with its accessories, which include the magnetometer sensor, sensor rod, control unit box, measuring tape, pegs, markers, and paper tags. The system consists of a 2 m long sensor rod, a coil-encased kerosene sensor cylinder, and a sensor connector. The kerosene sensor contains hydrogen dipoles enriched with free unpaired electrons. This highly sensitive magnetometer, with a precision of 0.1 nT, assists the acquisition of Total Magnetic Intensity (TMI) for the study. The field procedure for this technique requires the inspection of the area to enable the removal and/or avoidance of metallic objects or structures that might distort the local magnetic field during data acquisition in the study area. Prior to the commencement of the data acquisition, base station was established in order to serve as reference point for the data acquisition. It also aids in correcting diurnal variations in the Earth's magnetic field, thus enhancing

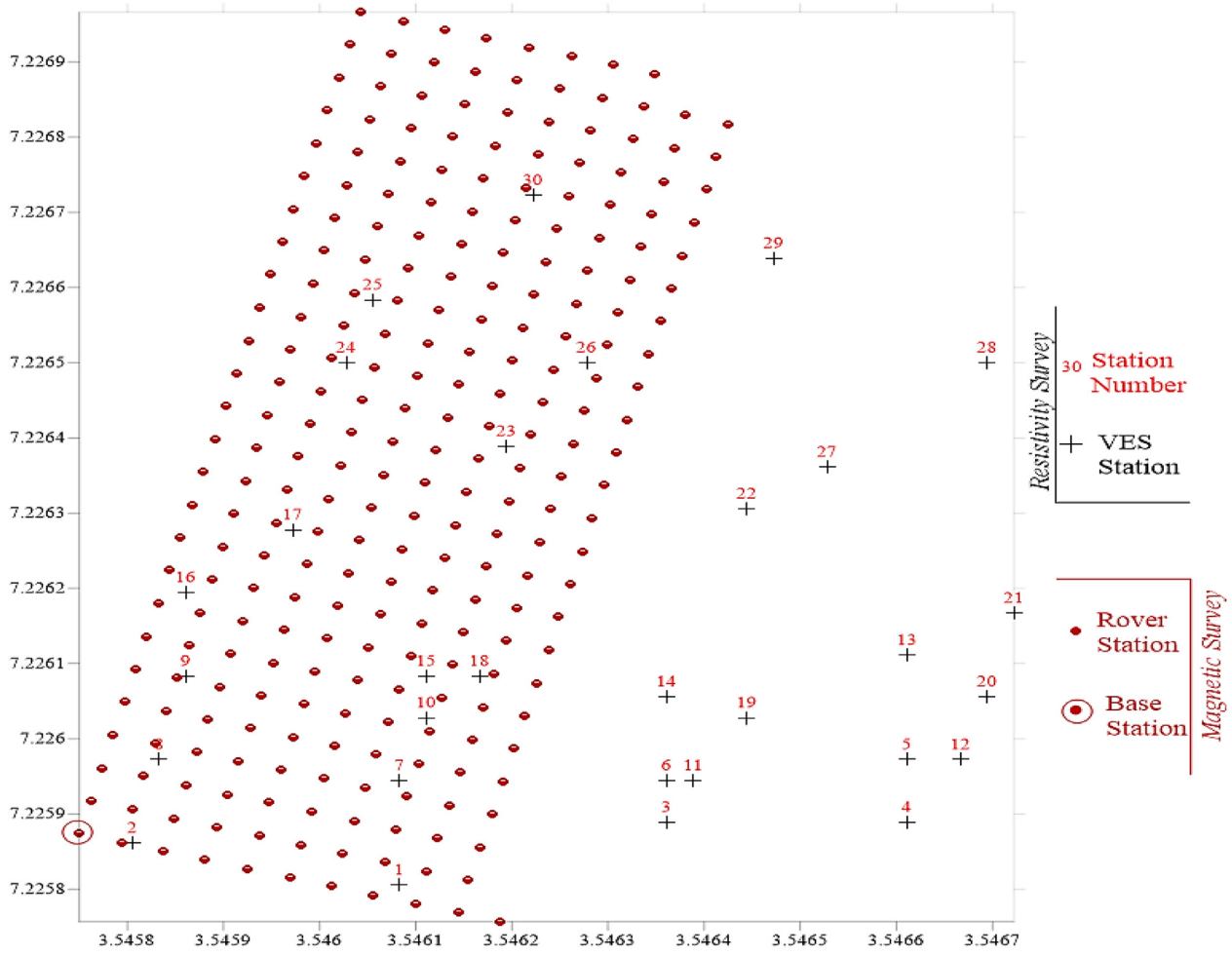

Fig. 3. Gridded basemap of the study area specifying the location of ER and ground.

the quality of the acquired data. This is followed by the gridding of the area, which was done at a station interval of 5 m using the Cartesian coordinate system as presented in Fig. 3. The first (base) reading was taken at the established base station noting the starting time of the survey. Magnetometer will then be moved to the next point for the acquisition of its Total Magnetic Intensity (TMI) reading. This process progressively advanced accordingly to all points until the last point in the grid is covered but however repeated measurements at the base station to keep track of diurnal changes.

2.3. Data processing

After magnetic data acquisition, the dataset undergoes essential preprocessing steps, including diurnal variation correction using base station measurements to account for temporal changes in the Earth's magnetic field. Additionally, the International Geomagnetic Reference Field (IGRF) is subtracted to remove regional magnetic influences, thereby isolating local magnetic anomalies associated with near-surface geological features. The corrected data is then filtered, gridded, and enhanced for better interpretation of anomaly maps and profiles, which are analyzed to estimate the depth and geometry of subsurface features [29,30]. The regional magnetic field was obtained from total magnetic field using low-order polynomial fitting. This method models long-wavelength, deep-source anomalies that are considered regional in nature. Once modeled, the regional component is subtracted from the original TMI dataset to obtain the residual magnetic field [30]. This step is essential for refining geologic models and improving the focus on anomalies caused by shallow magnetic sources such as ore bodies or structural features.

Magnetic data processing aimed at isolating subsurface magnetic anomalies from background magnetic signals that are not geologically relevant. It involves refining raw measurements in order to highlight subsurface geological feature through residual magnetic map. For this study, the residual magnetic map was generated by processing the acquired magnetic data using International Geomagnetic Reference Field (IGRF) correction and diurnal variation correction.

The diurnal variation correction addresses short-term temporal fluctuations in the Earth's magnetic field, caused by solar and ionospheric activities. These fluctuations are capable of distorting true magnetic signal of subsurface features if not corrected. To avert this, a base station was established during data acquisition at a stable location to record the natural variation of the geomagnetic field over time. The magnetic readings from this base station are time-matched and subtracted from the corresponding field data to remove diurnal influences [31,32]. This ensures that the magnetic anomalies observed in the data reflect spatial changes due to subsurface materials, not temporal noise.

The IGRF correction, on the other hand, removes the Earth's primary geomagnetic field—a global-scale, slowly varying magnetic field that does not relate to local geology. The IGRF is a mathematical model that estimates the Earth's main field based on time and location. By calculating IGRF values for the coordinates and date of each measurement and subtracting them from the raw magnetic intensity data, a residual magnetic field is obtained. The objective is to enhance short-wavelength anomalies through the removal of regional trends associated with deeper geological source [31,32].

The magnetic data was processed and interpreted using direct method. The direct method of interpreting magnetic data involves analyzing the acquired magnetic information to directly infer subsurface geological structures or features without extensive modeling or inversion. The method offers a qualitative understanding of subsurface features through visual inspection and basic calculations without the need for computational resources. Ref. [33] demonstrated the use of power spectrum for depth determination by graphically proving that the log-power spectrum with a linear gradient whose magnitude is dependent upon the source depth, thereby providing a rapid depth estimates from regularly spaced field data. A great advantage of this spectral analysis technique is that it does not dispense with the need for geomagnetic or diurnal correction since it removes only low wave number component.

Integrated electrical and magnetic methods significantly enhance mineral exploration by combining the high-resolution, shallow-depth imaging of electrical surveys with the deep structural mapping capabilities of magnetic techniques, ensuring more accurate targeting and efficient resource delineation [34–36].

3. Results and discussion

3.1. Geo-electric layers

The processed results of the acquired Vertical Electrical Soundings (VES) data are presented as obtainable in Table 1. The table illustrates the geoelectric parameters as obtained in each sounding points. The parameters include the delineated geo-

Table 1. Geo-electric parameters of the VES obtained in the study area.

VES Station	Layer number	Resistivity (Ωm)	Thickness (m)	Depth (m)	Reflection coefficient	Curve type	Inferred lithology
1	1	353	1.0	1.0	0.83	H	Topsoil
	2	48	4.3	5.3			Clay
	3	530	–	–			Fresh Basement
2	1	416	1.1	1.1	0.84	H	Topsoil
	2	53	5.2	6.3			Clay
	3	602	–	–			Fresh Basement
3	1	363	1.1	1.1	0.76	H	Topsoil
	2	127	4.7	5.8			Sandy Clay
	3	917	–	–			Fresh Basement
4	1	886	1.1	1.1	0.52	H	Topsoil
	2	181	7.3	8.4			Sandy Clay
	3	574	–	–			Fractured Basement
5	1	586	1.4	1.4	0.75	H	Topsoil
	2	97	6.1	7.5			Clay
	3	680	–	–			Fresh Basement
6	1	742	0.9	0.9	0.76	H	Topsoil
	2	78	4.3	5.2			Clay
	3	574	–	–			Fresh Basement
7	1	389	0.9	0.9	0.81	H	Topsoil
	2	65	5.1	6.0			Clay
	3	612	–	–			Fresh Basement
8	1	556	0.9	0.9	0.82	H	Topsoil
	2	59	5.6	6.6			Clay
	3	599	–	–			Fresh Basement
9	1	593	1.1	1.1	0.78	H	Topsoil
	2	65	10.8	11.9			Clay
	3	521	–	–			Fresh Basement
10	1	302	0.9	0.9	0.84	H	Topsoil
	2	67	5.6	6.5			Clay
	3	773	–	–			Fresh Basement
11	1	526	0.9	0.9	0.86	H	Topsoil
	2	72	5.0	5.9			Clay
	3	960	–	–			Fresh Basement
12	1	757	1.2	1.2	0.61	H	Topsoil
	2	144	8.5	9.7			Sandy Clay
	3	591	–	–			Basement
13	1	732	1.2	1.2	0.71	H	Topsoil
	2	161	9.0	10.2			Sandy Clay
	3	968	–	–			Fresh Basement
14	1	656	1.1	1.1	0.82	H	Topsoil
	2	93	5.4	6.5			Clay
	3	968	–	–			Fresh Basement
15	1	315	1.1	1.1	0.73	H	Topsoil
	2	67	6.3	7.4			Clay
	3	421	–	–			Fresh Basement
16	1	395	1.8	1.8	0.85	H	Topsoil
	2	59	8.5	10.3			Clay
	3	709	–	–			Fresh Basement
17	1	857	1.4	1.4	0.87	H	Topsoil
	2	91	9.9	11.2			Clay
	3	1357	–	–			Fresh Basement
18	1	302	1.0	1.0	0.79	H	Topsoil
	2	80	6.0	7.0			Clay
	3	680	–	–			Fresh Basement
19	1	459	1.3	1.3	0.72	H	Topsoil
	2	110	10.1	11.3			Sandy Clay
	3	665	–	–			Fresh Basement
20	1	484	1.2	1.2	0.68	H	Topsoil
	2	118	9.2	10.4			Sandy Clay
	3	626	–	–			Basement

(*continued on next page*)

Table 1. (continued)

VES Station	Layer number	Resistivity (Ωm)	Thickness (m)	Depth (m)	Reflection coefficient	Curve type	Inferred lithology
21	1	612	1.0	1.0	0.58	H	Topsoil
	2	120	7.6	8.7			Sandy Clay
	3	457	–	–			Basement
22	1	370	1.0	1.0	0.81	H	Topsoil
	2	110	6.0	7.0			Sandy Clay
	3	1020	–	–			Fresh Basement
23	1	933	1.2	1.2	0.78	H	Topsoil
	2	92	10.6	11.8			Clay
	3	753	–	–			Fresh Basement
24	1	666	1.9	1.9	0.81	H	Topsoil
	2	93	12.2	14.1			Clay
	3	879	–	–			Fresh Basement
25	1	824	1.7	1.7	0.81	H	Topsoil
	2	100	10.7	12.4			Clay
	3	959	–	–			Fresh Basement
26	1	455	1.1	1.1	0.82	H	Topsoil
	2	84	6.3	7.4			Clay
	3	852	–	–			Fresh Basement
27	1	525	1.0	1.0	0.84	H	Topsoil
	2	88	6.3	7.3			Clay
	3	991	–	–			Fresh Basement
28	1	313	1.3	1.3	0.87	H	Topsoil
	2	64	6.3	7.6			Clay
	3	897	–	–			Fresh Basement
29	1	457	1.2	1.2	0.83	H	Topsoil
	2	76	6.9	8.1			Clay
	3	834	–	–			Fresh Basement
30	1	901	1.6	1.6	0.82	H	Topsoil
	2	74	8.6	10.2			Clay
	3	739	–	–			Fresh Basement

electric layers with their corresponding resistivity values, thickness and the inferred lithology.

The interpretation of the acquired VES in the study area revealed that all sounding points are uniquely H curve type. This indicates the delineation of three (3) geo-electric layers characterized to comprise of resistive topsoil, underlain by an earth material of lower resistivity which is in turn underlain by a high resistive geologic material as described in Table 1. The resistivity values outlined from the delineated geo-electric layers ranges between 302 and 933 Ωm, 48–181 Ωm and 421–1357 Ωm representing the topsoil, weathered layer and the fresh bedrock. The topsoil as revealed by its resistivity range is largely made up of sand coupled with sparse occurrences of clayey sand; resistivity range of the weathered unit is characteristically reflective of clay and sandy clay heterogeneity. As a complementation to the generally high bedrock resistivity, the reflection coefficient values ranging from 0.52 to 0.87 discriminated between the fresh basement zone and the minor fractured spots. Bedrock topography generally warps northerly from the south as presented in the geo-electric section.

3.2. Geo-electric section

Geo-electric section shows the graphical description of the subsurface electrical resistivity as obtained from the processed VES data. It presents the lithological sequence of sounding points obtained along the same traverse line as shown in Fig. 4. The figure illustrates the extent and varying thickness of the each delineated formation on the same traverse line. The figure describes the depth to the basement thereby giving the details of the overburden decribed along each traverse line.

The number of layers inferred from the thirty (30) VES points in the study area as shown in Fig. 4 are depictions of geo-electric sections along the NE–SW and N–S directions. Along the NE–SW direction, the resistivity values range of the three geo-electric layers is 313–416 Ωm, 53–110 Ωm and 417–1020 Ωm for the topsoil (composed of clayey sand), weathered unit of (clay and sandy clay) and bedrock respectively. The overburden thickness values estimated along this traverse varies between 6.3 and 7.6 m from Southwest to Northeast with respect to the fresh basement topography (Fig. 4). Correspondingly, the resistivity values delineated

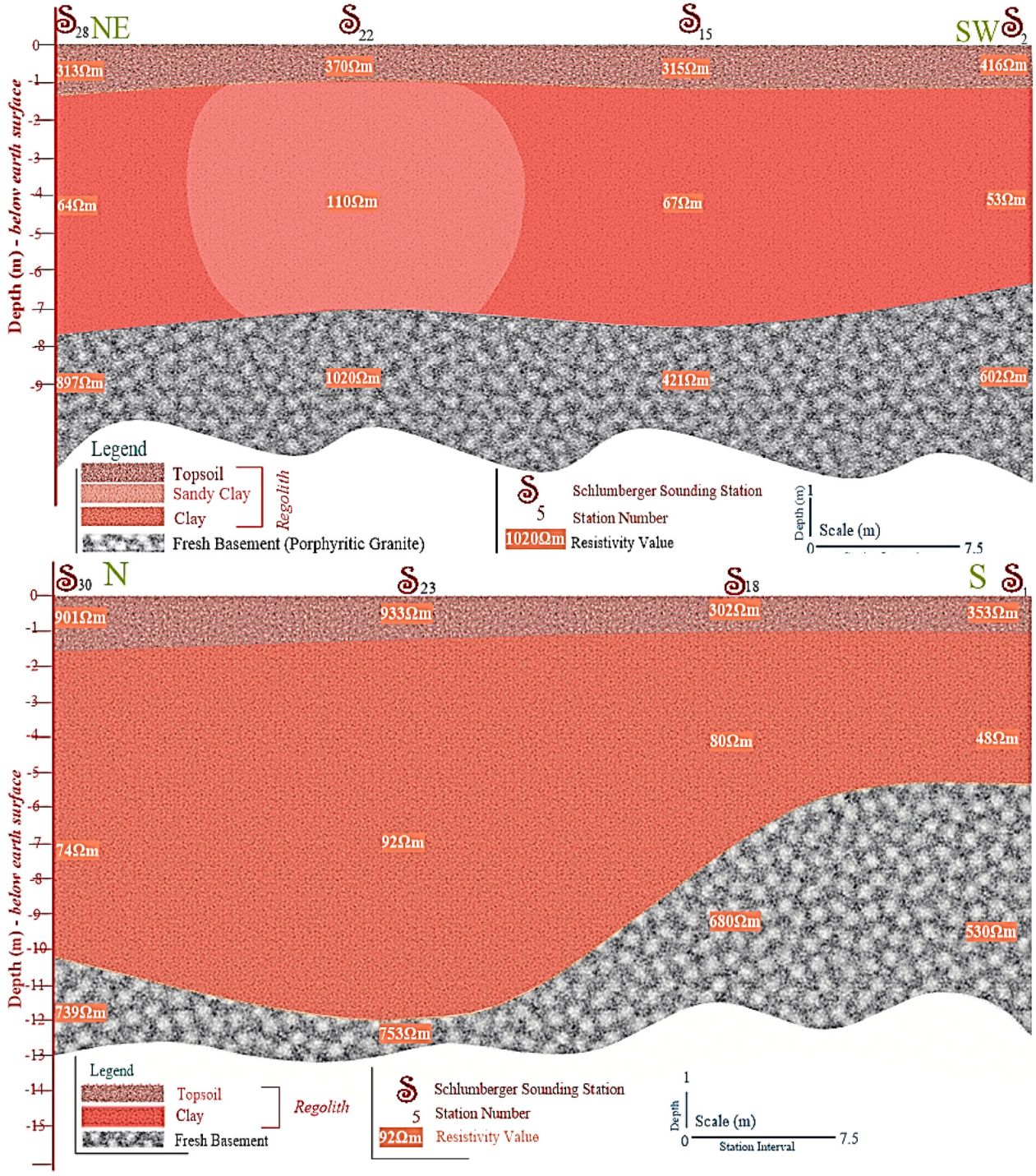

Fig. 4. Geo-electric section obtained from ER data.

along the N–S direction ranges from 302 to 933 Ωm, 48–92 Ωm, 530–753 Ωm for the topsoil, weathered unit and the fresh basement respectively. It was observed that the delineated topsoil differed compositionally; solely made up of sand in the northern part but composed of clayey sand down south. The weathered layer on the other hand is a homogeneous unit wholly composed of clay. The thickness values for the overburden are in range of 5.2 m in the South and 10.2 m towards the northern part of the traverse.

4. Magnetic data results

The distribution of the magnetic strength of the Earth's magnetic field in the study area is presented

as Total Magnetic Intensity (TMI) in Fig. 5. The contour map describes the spatial variation of the magnetic intensity as obtainable in the study area from the Earth's core sources and external sources. However, the Residual Magnetic Intensity (RMI) represents the measure of the magnetic field attributed to the induced and remnant magnetization of subsurface lithology after the removal of

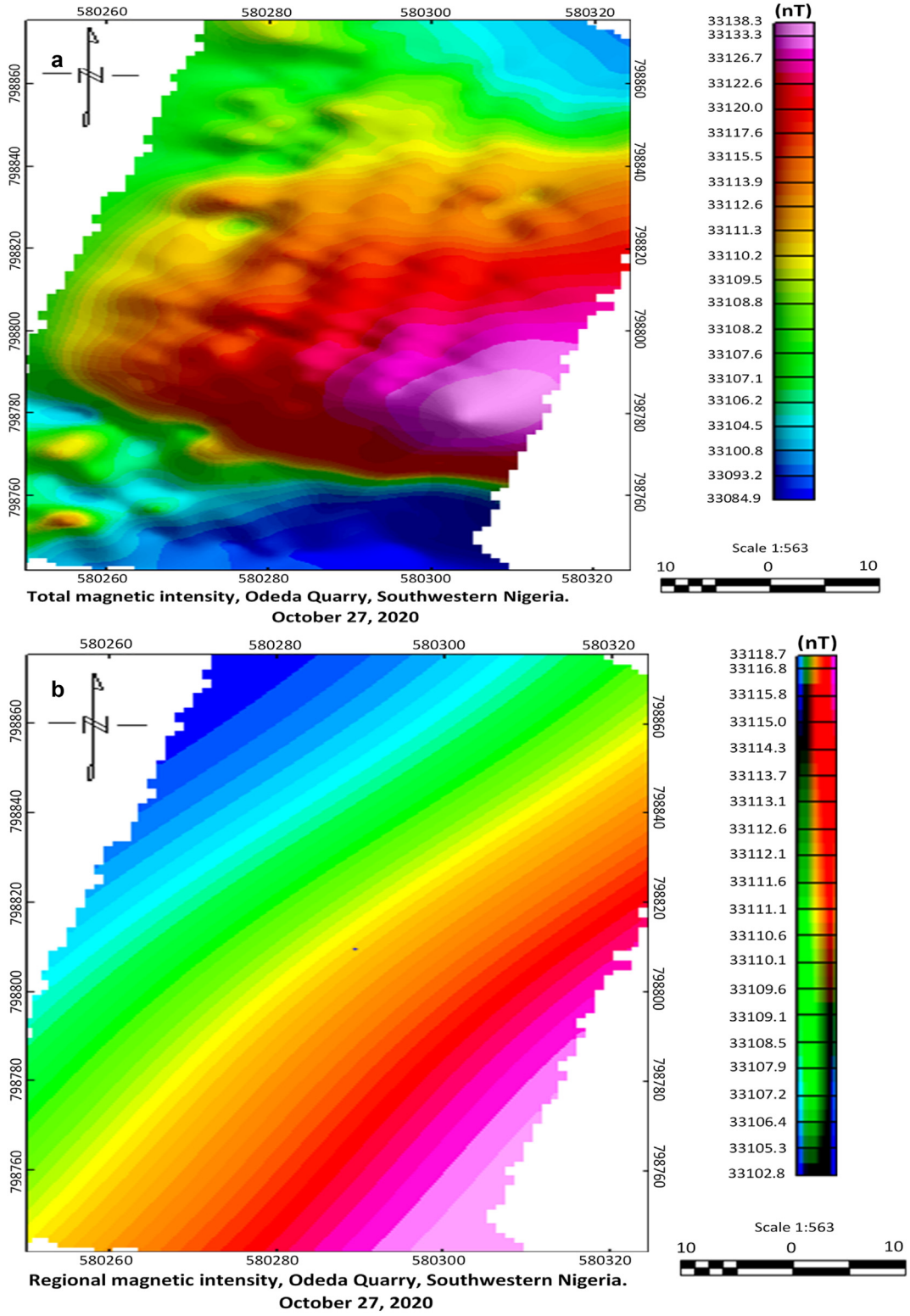

Fig. 5. The representation of (a) Total Magnetic Intensity (b) Regional Magnetic Intensity obtained from the study area.

regional and external field effects. The interpretation of RMI aids the assessment of the basement rock in the study area concerning its mineral deposits, fault lines, and other geological features. The described anomalies in RMI connote the characterization of the magnetic susceptibility distribution within the crystalline basement, thereby aiding inferences about the spatial relationships between magnetic signatures, subsurface features, and geological structures.

Total Magnetic Intensity (TMI) obtained from the study area ranges between 33,085 and 33,138 nT (Fig. 5a). Varying magnetic strengths were observed at the southern part of the delineated TMI. The Residual Magnetic Intensity (Fig. 6) outlined from the processed data range from −32 to 23 nT unravelling poor magnetic susceptibility from the magnetic source. The outlined poor magnetic susceptibility symbolizes as the presence of low magnetic igneous rock such as porphyritic granite (with quartz phenocryst). Three magnetic districts are recognizable, viz.; the null anomaly district (−3 to 3 nT) covering the Northern and Southwestern part, the large central weak positive anomaly (7.3–12.4 nT) contorted by pointed closure (17.7–22 nT), and the negative anomaly zone at the southeastern edge. Differences in the residual magnetization across the three districts do not necessarily connote any compositional changes but a reflection of depth variation of a single source. The depth of the magnetic source derived from the study area varies between 1 and 14 m, indicating the estimated overburden thickness as determined by the magnetic method. Consequently, the depth to the top of the identified porphyritic granite deposit falls within the range of 1–14 m.

The Fig. 7a and b illustrate the Euler deconvolution of the magnetic anomaly results. This method estimates the source location and depth from magnetic field gradients, accepted as a recent approach for identifying structural boundaries and lithological contacts [37–39]. Fig. 7a and b indicate that the depth of magnetic source bodies ranges from 1 to 14 m, with suspected porphyritic granite intrusions forming part of the basement complex.

The results reveal a varied depth distribution across the study area. The northern region displays shallow magnetic sources with depth ranges of 1–5 m, delineating weathered cover and basement rocks, suggesting a possible presence of porphyritic

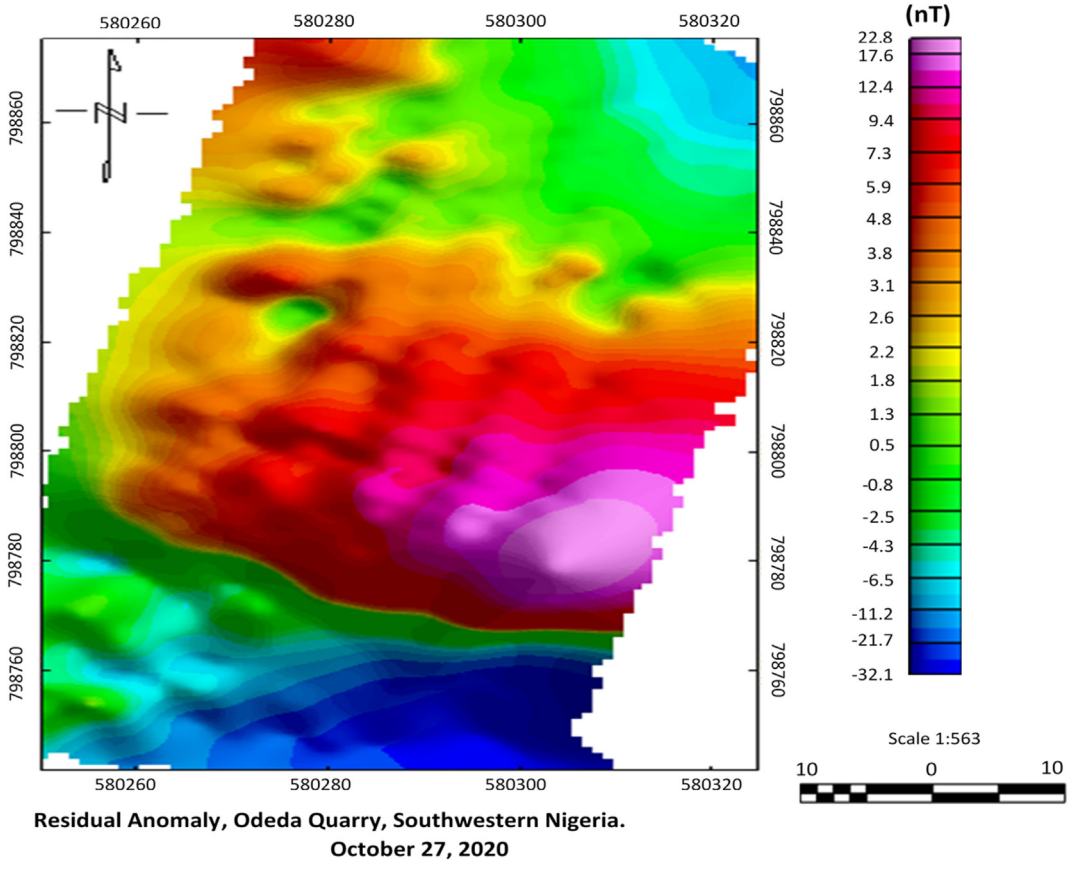

Fig. 6. The representation of Residual Magnetic Intensity obtained from the study area.

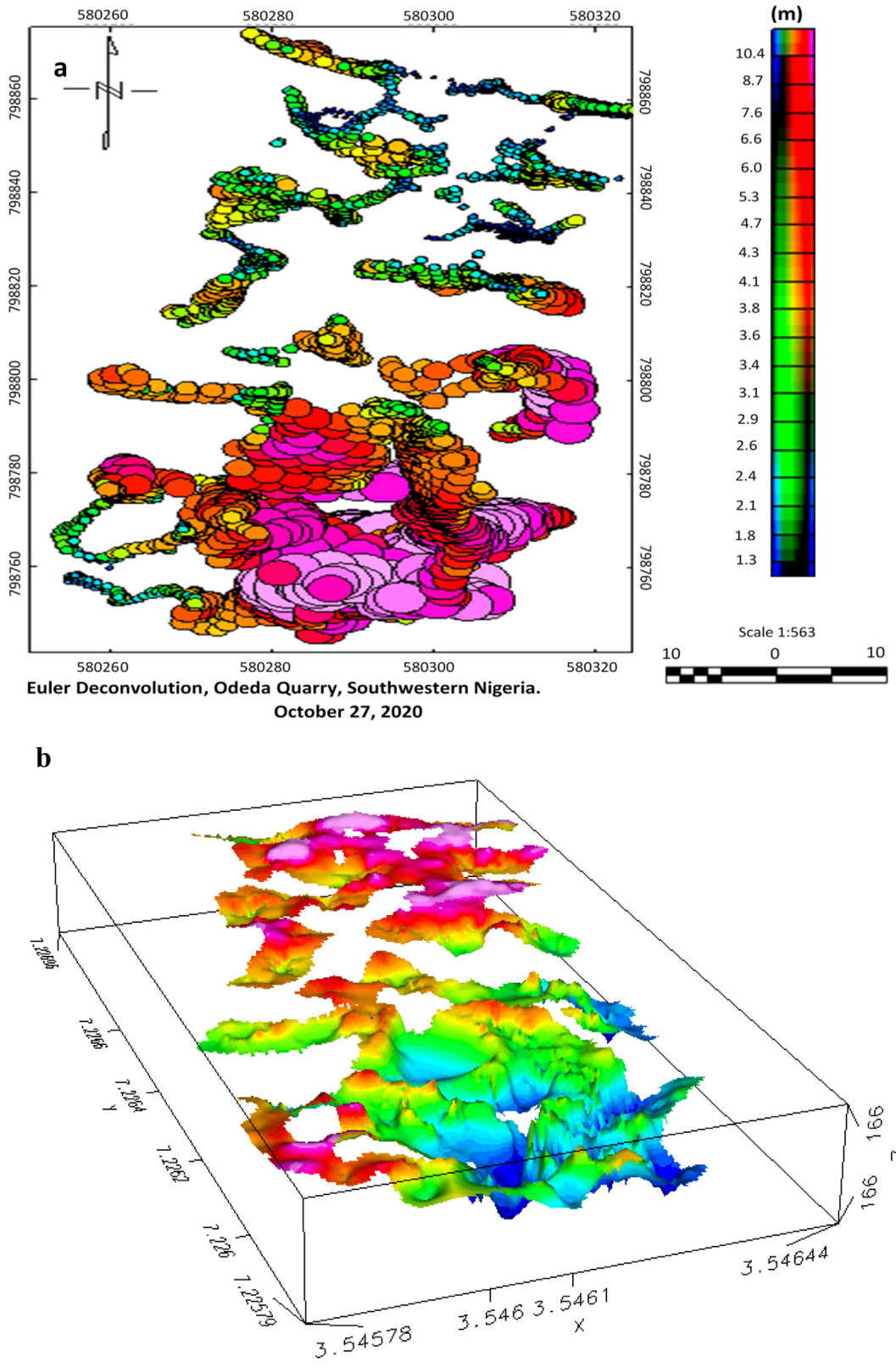

Fig. 7. The representation of Euler Deconvolution (a) Depth Model (b) Elevation Model.

granite near the subsurface. Similarly, the southern region uncovers a thick overburden with depths ranging from 6 to 14 m, likely consisting of alluvial deposits and weathered material. The figure indicates variations in subsurface structure and potential mineralization zones, with findings that align with current geophysical mapping trends in crystalline terrains, where depth-to-basement estimation supports mineral exploration studies [40].

4.1. Overburden thickness map

The overburden thickness delineated from the VES data were presented as Isopach map with respect to the coordinates (Fig. 8). The isopach map illustrates the thickness of the delineated minerals with their stratigraphical interval. This was achieved through the connection of overburden thickness contour lines of equal thickness allowing easy visualization of the distribution and variation in thickness of the unraveled minerals and basement.

The overburden thickness outlined in the study area as presented in Fig. 8 varies between 6.5 and 13 m. The study area was gridded with dimension of about 0.0625 km^2 for each grid. Sixteen (16) grids of 4 by 4 were used for the Isopatch distribution of the overburden thickness. High thicknesses ranging from 9.5 to 13.0 m were delineated towards the NW of the study. This implies that high regolith accumulation will be encountered in the described portions. However, the NE-SW portions of the gridded portion displayed the presence of low regolith and high reserve as presented in Fig. 9.

The estimated volume from the outlined grid described more prospective grid as presented in Table 2. The expected volume of the prospective portions varies from 4062.5 to 53,125.5 m^3. The estimated prophylactic potential obtained from the table affirmed the overburden and regolith ratio described in regolith/reserve chart (Fig. 9). The distributions of the abundance of the minerals as obtained from the established grip are concentrated along NE–SW direction of the study area. The mineral potentials are more prolific along the northern–southern part of the study area.

The poor magnetic responses recorded at the near-surface in the northern part depict the presence of magnetite bearing sources. These observations are symptomatic that the rocks are with felsic components of the basement complex. However, anomalous low susceptibility within the migmatite

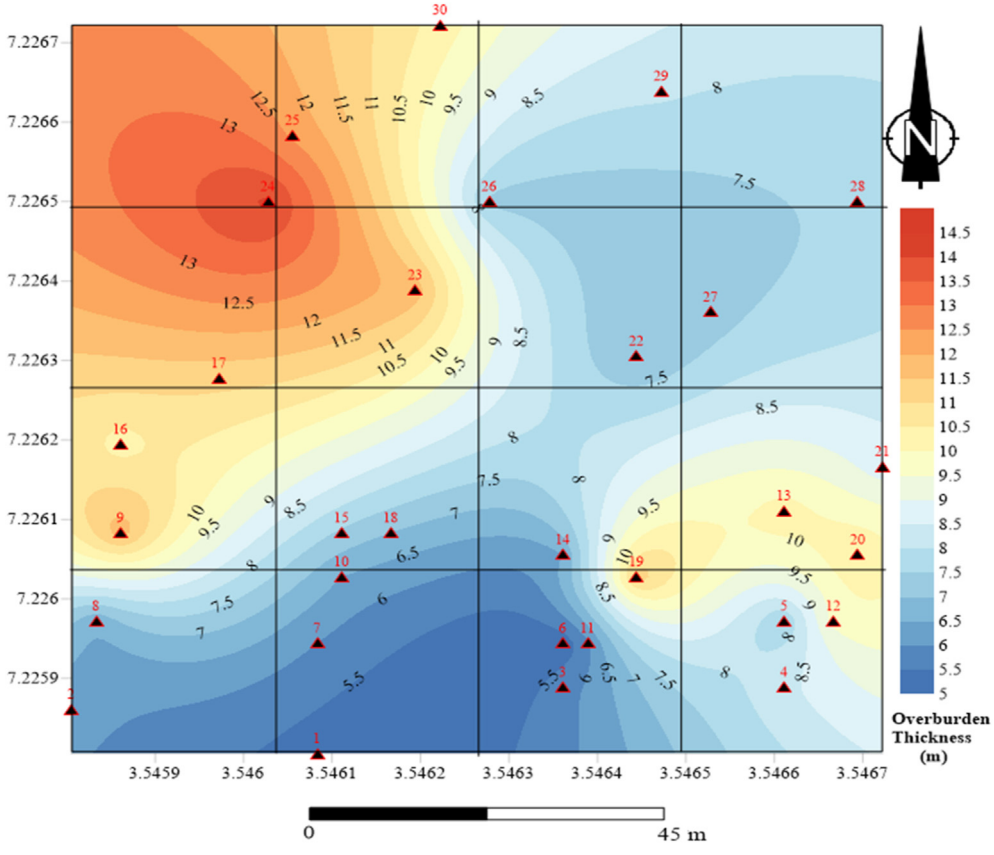

Fig. 8. Isopach Map showing the overburden thickness with embedded VES points.

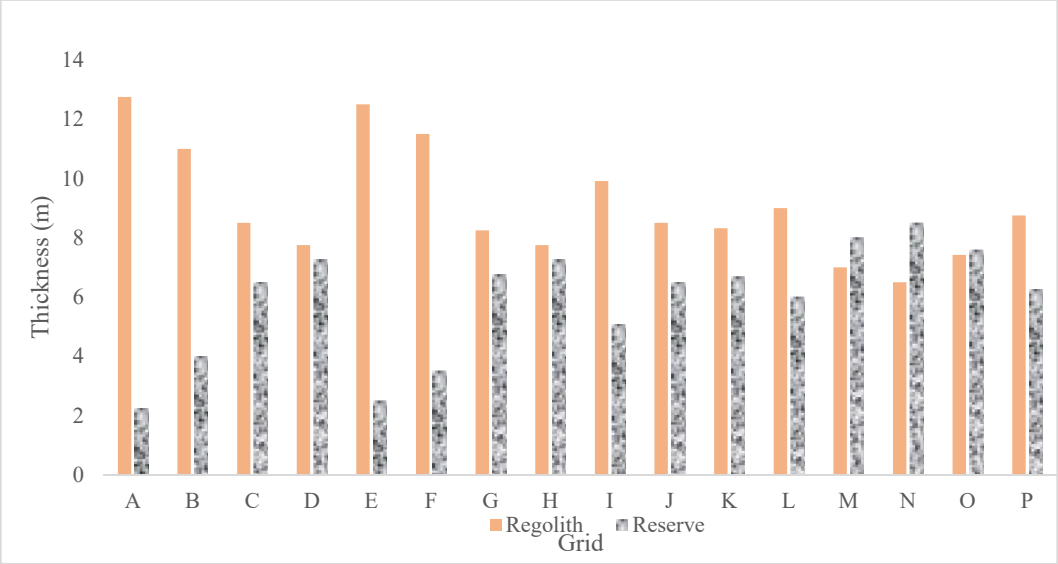

Fig. 9. Regolith and reserve (rock) thickness distribution across the grids.

body is not an indication of fractures but a reflection of depth variation which trends in multi-directional in the Northeast–Southwest, North–West. It is worthy to note that the northern part is apparently the most prolific with appreciable magnetic minerals (granite) which are naturally found in association with ferromagnesian.

4.2. Bulk tonnage distribution

For optimum evaluation of the mineral potential, the non-prospective grid locations (covered by excessive regolith) required to be classified from the delineated points. The classification enhances the efficiency of exploration by concentrating efforts on areas with viable mineral deposit exposure. To estimate the tonnage of the mineral deposit in each grid, a calculation model incorporating basic parameters was employed: the area dimension of the grid, average overburden thickness, a benchmark depth (baseline) for mineral estimation, average reserve thickness, and the specific gravity of the porphyritic granite deposit. These variables allow for a volumetric and mass-based computation of in-place reserves. The estimated bulk tonnage is presented using a bar chart (Fig. 9), which distinguishes the reserve rock (granite with mineral potential) and the regolith overburden

Table 2. Estimation parameters for the bulk estimation of mineral potential.

Grid	Average Overburden Thickness (m)	Average Depth To Basement (m)	Average Reflection Coefficient	Rock Thickness (m)	Area Dimension Of Grid (m^2)	Volume (m^3)	Specific Gravity	Remark
A	12.75	12.75	0.83	2.25	625	1406.25	2.69	NP
B	11	11	0.82	4	625	2500	2.69	NP
C	8.5	8.5	0.83	6.5	625	4062.5	2.69	P
D	7.75	7.75	0.85	7.25	625	4531.25	2.69	P
E	12.5	12.5	0.84	2.5	625	1562.5	2.69	NP
F	11.5	11.5	0.81	3.5	625	2187.5	2.69	NP
G	8.25	8.25	0.82	6.75	625	4218.75	2.69	P
H	7.75	7.75	0.79	7.25	625	4531.25	2.69	P
I	9.91	9.91	0.82	5.09	625	3181.25	2.69	NP
J	8.5	8.5	0.79	6.5	625	4062.5	2.69	P
K	8.32	8.32	0.79	6.68	625	4175	2.69	P
L	9	9	0.7	6	625	3750	2.69	P
M	7	7	0.81	8	625	5000	2.69	P
N	6.5	6.5	0.8	8.5	625	5312.5	2.69	P
O	7.42	7.42	0.75	7.58	625	4737.5	2.69	P
P	8.75	8.75	0.64	6.25	625	3906.25	2.69	NP

Key: P - Prospective Grid; NP - Non Prospective Grid.

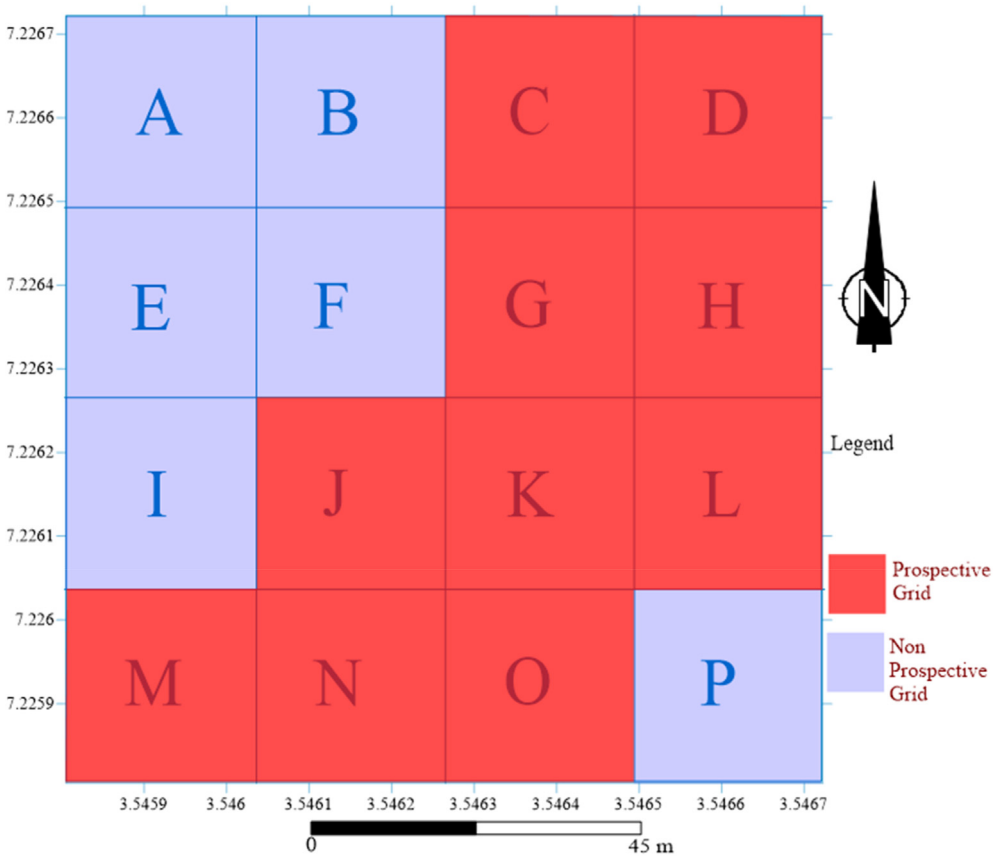

Fig. 10. Prospective distribution delineated from Resistivity Section in the Study area.

thereby providing a comparative representation of prospective versus non-prospective points/grid. The estimation parameters used for these calculations are detailed in Table 2, from which the classification of prospective and non-prospective grid points (as shown in Fig. 10) was derived. The procedure and comparison deployed for this study are increasingly applied in mineral resource evaluation, particularly in basement complex terrains [30,31,38].

5. Conclusion

The integrated approach of Magnetic and Electrical resistivity methods has successfully outlined the depth to basement and the distribution of the prospective minerals in the study area. The electrical resistivity method illustrated three geo-electric layers with resistivity values spanning from 313 to 416 Ωm, 53–110 Ωm and 417–1020 Ωm describing the topsoil (composed of clayey sand), weathered unit of (clay and sandy clay) and bedrock respectively. The topsoil delineated are found to be differed compositionally thereby solely made up of sand in the Northern part but composed of clayey sand down Southern of the investigated area. On the other hand, the weathered layer comprises of a homogeneous unit wholly composed of clay. The thickness range of overburden outlined varies from 5.2 to 10.2 m in the study area.

Similarly, the processed magnetic data showed variation in the magnetic field strength outlined in the area, the southern part of the investigated area showed both minimum and maximum field strength. The irregular range in the residual strength showed the presence of poor susceptibility characteristic of the magnetic source(s) – which in this stance, can be inferred as the mapped porphyritic granite (with quartz phenocryst). Although, three (3) magnetic districts were outlined, namely; the null anomaly district with average residual strength that varies from −3 to 3 nT dominating the Northern and Southwestern part. Also, the large central weak positive anomaly with magnetic field strength of 7.3–12.4 nT contorted by pointed closure, and the negative anomaly zone at the Southeastern edge. The variation in the residual magnetization across the three districts does not necessarily connote any compositional changes but a reflection of depth variation of a single source.

However, the depth of magnetic source varied between 1 and 14 m. Since the source bodies is invariably basement rocks, then the depth to the top of the porphyritic granite deposit ranges between 1 and 14 m. Two pattern of depth distribution are apparent on the Euler convolution plot, which reclassified the area into; the shallow northern part with a depth range between 1 and 5 m, and the overburden-covered southern part with thickness generally ranging between 6 and 14 m.

Source of Funding

This research received no external funding.

Conflict of Interest

The authors do not have any conflict of interest to declare.

Ethical Approval

The manuscript has not been published or submitted for publication by any other journal. The findings presented in the manuscript are original.

Data Availability

The data supporting the findings of this study are presented in the manuscript. The raw datasets or analysis outputs are available on request.

Author Contributions

HTO: Conceptualization, analysis of results reviewed and attending to manuscript correspondence; JC: methodology, analysis of results and review the initial draft; N-OA: reviewing of relevant literatures, methodology and analysis of results; OAA: acquisition and processing of Magnetic Data; acquisition and processing of electrical resistivity data; SAA: acquisition and analysis of the data results; AA: Acquisition, processing of results, drafting the initial report. All authors reviewed and edited the manuscript and approved the final version.

Acknowledgement

The authors are grateful to the district head for the permission granted during the field work exercise. Likewise, the anonymous reviewers that reviewed the manuscript.

References

[1] Ehinola OA, Oladunjoye MA, Gbadamosi TO. Chemical composition, geophysical mapping and reserve estimation of clay deposit from parts of Southwestern Nigeria. J Geol Min Res 2009;1(3):57–66.
[2] Joshua EO, Oladunjoye MA, Bayewu OO. Mapping structure using combined seismic refraction and electrical resistivity methods: a case study of Omi-Adio overburden and its environs, south western Nigeria. Afr Geosci Rev 2004;11(4):281–91.
[3] Yavuz AB, Turk N, Koca MY. Geological parameters affecting the marble production in the quarries along the southern flank of the Menderes Massif, in SW Turkey. Eng Geol 2005;80(3–4):214–41.
[4] Butler DK. Near earth surface geophysics. Society of exploration geophysicists; 2005. p. 758.
[5] Olorunfemi MO, Okhue ET. Hydrogeologic and geologic significant of a geoelectric survey at Ile-Ife, Nigeria. J Min Geol 1992;28(2):221–9.
[6] Bayewu OO, Oloruntola MO, Mosuro GO, Olagunju O. Determination of groundwater potential of an area using electrical resistivity method: a case study of Olabisi Onabanjo University Mini Campus. Afr J Pure Appl Sci 2008;2(1):17–23.
[7] Kröner A, Stern RJ. Pan-African orogeny. Encycl Geol 2005;1:1–12.
[8] Goodenough KM, Lusty PAJ, Roberts NMW, Key RM, Garba A. Post-collisional Pan-African granitoids and rare metal pegmatites in western Nigeria: age, petrogenesis, and the 'pegmatite conundrum. Lithos 2014;200:22–34.
[9] Akanbi ES, Ugodulunwa Fx Gyang BN. 2-D electrical resistivity survey for cassiterite potential mapping in Jos-Bukuru Area, North Central, Nigeria. J Geogr Environ Earth Sci Int 2017;10(1):1–12. https://doi.org/10.9734/JGEESI/2017/33350.
[10] Arifin MH, Kayode JS, Izwan MK, Zaid HAH, Hussin H. Data for the potential gold mineralization mapping with the applications of Electrical Resistivity Imaging and Induced Polarization geophysical surveys. Data Brief 2019;22:830–5.
[11] Layade GO, Edunjobi HO, Ajayi KD. Lineament, qualitative interpretation and depth evaluation of potential field signatures in the Abeokuta Region, Southwestern Nigeria. J Earth Space Phys 2024;49(4).
[12] Popoola OI, Adenuga OA, Joshua EO. Ground magnetic survey for the investigation of magnetic minerals at Iboro Village, Abeokuta, South-Western Nigeria. Sci Africana 2021;20(2):99–106.
[13] Edunjobi HO, Layade OG, Makinde V, Bada BS, Ogunbayo AF, Atunrase KA. Qualitative interpretation of high resolution aeromagnetic data of Abeokuta metropolis for geological characterisation. Res Geophys Sci 2023;15:100062.
[14] Ojo A, Adeloye M, Egbedele I, Akinwande F. Magnetic rocks distribution and depth to basement analysis on an old quarry site, Abeokuta, SW Nigeria. Iran J Earth Sci 2020;12(3):176–83.
[15] Abubakar HO, Raji WO, Bayode S. Direct current resistivity and very low frequency electromagnetic studies for groundwater development in a basement complex area of Nigeria. Sci Focus 2014;19(1):1–10.
[16] Aromoye SA, Alimi SA, Bello OS, Raji WO, Olawale LO, Bonde SD. 2-D electrical resistivity tomography for groundwater potential in basement terrain of a part of Ilorin Sheet 223 NW Nigeria. Saudi J Eng Technol 2019;4:357–62. https://doi.org/10.36348/SJET.2019.v04i09.004.
[17] Ibrahim A, Toyin A, Sanni ZJ. Geological characteristics and petrographic analysis of rocks of Ado-Awaiye and its Environs, Southwestern Nigeria. Int J Appl Sci Math Theory 2015;1(8):28–47.
[18] Abdulbariu I, Bala A. Geomagnetic signature and depth estimate of basement rock around iseyin area (Ado-Awaiye), Ibadan, Southwestern Nigeria. J Geogr Environ Earth Sci Int 2016;4(2):1–12.
[19] Sedera SO, Alabi OO, Akinwande DD. Depth estimation of mineral deposit using magnetic method in Oduduwa University, Ipetu Modu, Southwestern Nigeria. FUTA J Res Sci 2016;12(2):325–33.

[20] Onyedim GC, Awoyemi MO. Integration of enhanced horizontal derivative filtering and shaded relief display as aid to lineament mapping on potential field images. IFE J Sci 2005; 7(2):253−61.
[21] Kayode JS, Adelusi AO. Ground magnetic data interpretation of Ijebu-Jesa area, Southwestern Nigeria, using total component. Res J Appl Sci Eng Technol 2010;2(8):703−9.
[22] Adagunodo TA, Sunmonu LA, Adabanija MA. Geomagnetic signature pattern of industrial layout Orile Igbon. Adv Archit City Envi 2015;1(3):14−25.
[23] Solanke MO. Spatial pattern and organisational structure of intra-urban trips in Ogun State, Nigeria. Ethiop J Environ Stud Manag 2015;8(1):13−27.
[24] Salami BM, Olorunfemi MO. Hydrogeophysical evaluation of the groundwater potential of the central part of Ogun State, Nigeria. IFE J Sci 2014;16(2):291−9.
[25] Olayinka AI. Non-uniqueness in the interpretation of bedrock resistivity from sounding curves and its hydrological implications. Water Resour J NAH 1996;7(1&2):55−60.
[26] Okurumeh OK, Olayinka AI. Electrical anisotropy of crystalline basement rocks around Okeho, southwestern Nigeria: implications in geologic mapping and groundwater investigation. Water Resour J NAH 1998;9:41−50.
[27] Oyinloye AO, Obasi RA. Geology, geochemistry, and geotectonic setting of the Pan-African granites and charnockite around Ado-Ekiti, southwestern Nigeria. Pak J Sci Ind Res 2006;49(5):299−308.
[28] Al-Garni M. Magnetic and DC resistivity investigation for groundwater in a complex subsurface terrain. Arabian J Geosci 2011;4:385−400.
[29] Abdelazeem M, Gobashy MM. A solution to unexploded ordnance detection problem from its magnetic anomaly using Kaczmarz regularization. Interpretation 2016;4(3): SH61−S69.
[30] Ozegõn KO, Alõle OM. Exploit of ground magnetic survey data for solid mineral exploration. Int J Earth Sci Knowl Appl 2021;3(3):208−16.
[31] Lawali S, Salako KA, Bonde DS. Delineation of mineral potential zones over lower part of Sokoto Basin, northwestern Nigeria using aeromagnetic data. Acad Res Int 2020;11(2): 19−29.
[32] Okpoli Cyril C. Ground magnetic prospecting of precambrian basement rocks of Ayegunle-Oka, Supare-Akoko and Akungba-Akoko, southwestern Nigeria. Indian J Sci 2017; 24(93):469−83.
[33] Spector A, Grant FS. Statistical models for interpreting aeromagnetic data. Geophysics 1970;35(2):293−302.
[34] Oldenburg DW, Pratt DA. Geophysical inversion for mineral exploration: a decade of progress in theory and practice. Proc Explor 2007;7(5):61−95.
[35] Ugbor CC, Emedo CO, Arinze IJ. Interpretation of airborne magnetic and geo-electric data: resource potential and basement morphology of the Ikom−Mamfe Embayment and Environs, Southeastern Nigeria. Nat Resour Res 2021;30: 153−74.
[36] Adelusi AO, Kayode JS, Akinlalu AA. Interpretation of aeromagnetic anomalies and electrical resistivity mapping around Iwaraja area Southwestern Nigeria. J Geol Min Res 2013;5(2):38−57.
[37] Keating P, Pilkington M. Euler deconvolution of the analytic signal and its application to magnetic interpretation. Geophys Prospect 2004;52(3):165−82.
[38] Githiri JG, Patel JP, Barongo JO, Karanja PK. Application of Euler deconvolution technique in determining depths to magnetic structures in Magadi area, southern Kenya Rift. J Agric Sci Technol 2011;13(1):142−56.
[39] Usman N, Abdullah K, Nawawi M, Khalil AE. New approach of solving Euler deconvolution relation for the automatic interpretation of magnetic data. Terr Atmos Ocean Sci 2018; 29:243−59.
[40] Okechukwu PN, Ofuyah WN, Oguh AM. Basement depths estimation using the Euler-3D and source parameter imaging methods from the analysis of ground magnetic field data in the Niger Delta Basin. Int J Sci Res Arch 2025;14(1):218−29.